ACS NANO

www.acsnano.org

ARTICLE

A Solution Processable Dithioalkyl Dithienothiophene (DSDTT) Based Small Molecule and Its Blends for High Performance Organic Field Effect Transistors

Chia-Chi Lin,[¶] Shakil N. Afraj,[¶] Arulmozhi Velusamy, Po-Chun Yu, Chang-Hui Cho, Jianhua Chen, Yi-Hsien Li, Gene-Hsiang Lee, Shih-Huang Tung, Cheng-Liang Liu,* Ming-Chou Chen,* and Antonio Facchetti*

Cite This: *ACS Nano* 2021, 15, 727−738

Read Online

ACCESS | Metrics & More | Article Recommendations | Supporting Information

ABSTRACT: The 3,5-dithiooctyl dithienothiophene based small molecular semiconductor DDTT-DSDTT (1), end functionalized with fused dithienothiophene (DTT) units, was synthesized and characterized for organic field effect transistors (OFET). The thermal, optical, electrochemical, and computed electronic structural properties of 1 were investigated and contrasted. The single crystal structure of 1 reveals the presence of intramolecular locks between S(alkyl)···S(thiophene), with a very short S−S distance of 3.10 Å, and a planar core. When measured in an OFET device compound 1 exhibits a hole mobility of 3.19 $cm^2\ V^{-1}\ s^{-1}$, when the semiconductor layer is processed by a solution-shearing deposition method and using environmentally acceptable anisole as the solvent. This is the highest value reported to date for an all-thiophene based molecular semiconductor. In addition, solution-processed small molecule/insulating polymer (1/PαMS) blend films and devices were investigated. Morphological analysis reveals a nanoscopic vertical phase separation with the PαMS layer preferentially contacting the dielectric and 1 located on top of the stack. The OFET based on the blend comprising 50% weight of 1 exhibits a hole mobility of 2.44 $cm^2\ V^{-1}\ s^{-1}$ and a very smaller threshold voltage shift under gate bias stress.

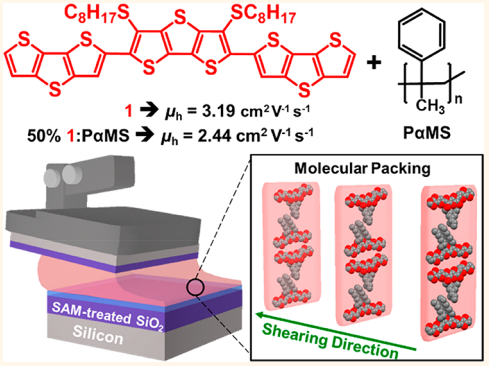

KEYWORDS: *organic semiconductors, organic transistor, 3,5-dithioalkyl dithienothiophene, solution-processing, polymer blend*

Organic semiconductors have attracted tremendous attention because of their advantageous mechanical flexibility that they inherently possess; thus, organic electronic devices are expected to open applications, such as flexible displays, smart cards, sensors, storage devices, radio frequency tags, and transparent circuits[1−13] as well as be utilized in biomedical applications such as large-area sensitive catheters.[14] Hence, the realization of π-conjugated small molecule and polymeric materials has received much attention.[15−25] The design of solution processable small molecule semiconductors with good charge transport characteristics, particularly in organic field-effect transistors (OFETs), relies on structural design possessing a planar conjugated backbone to enhance molecular stacking via intermolecular orbital overlap, functionalized with suitable side chains for easy solution processability and exhibiting good environmental stability.[26−29] To this end, several π-conjugated structures have been developed,[30] and among them, *n*-(hetero)acenes (particularly n = 4−7) are important building blocks for organic electronics because they exhibit highly planar structures, extended conjugation, and, when sulfur is present, strong intermolecular S···S interactions.[19,20,30−34] Despite these advantages there are some drawbacks including the poor chemical stability of several *n*-acenes (n > 3) (Figure 1a), difficult synthesis particularly for fused (thio)acenes with *n*

Received: August 20, 2020
Accepted: November 23, 2020
Published: November 30, 2020

https://dx.doi.org/10.1021/acsnano.0c07003
ACS Nano 2021, 15, 727−738

> 5, and limited solubility which impacts the film morphological quality.[35−37]

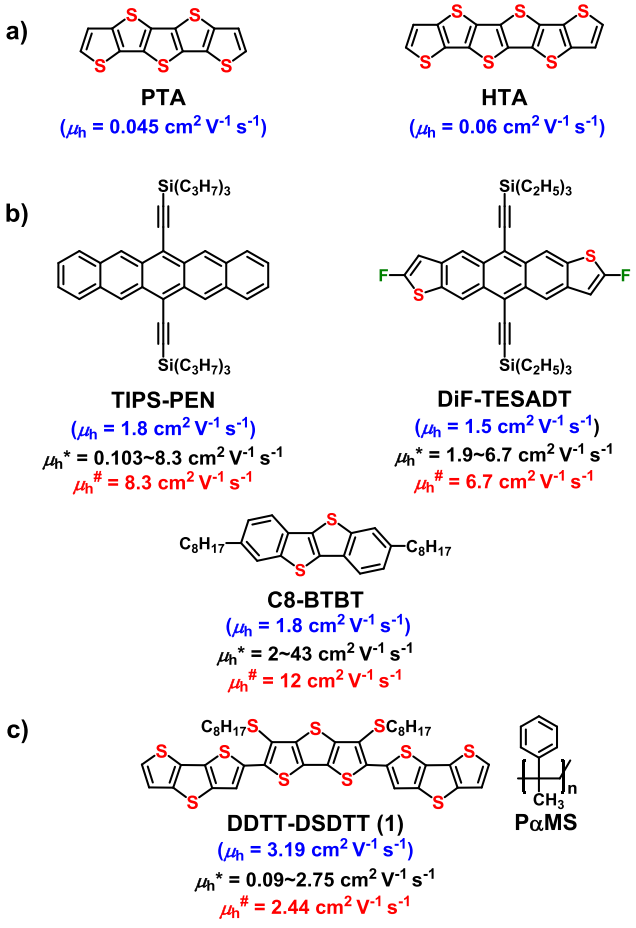

Figure 1. Chemical structures of (a) fused (thio)acenes PTA and HTA, (b) TIPS-PEN, DiF-TESADT, C8-BTBT, and (c) DDTT-DSDTT (1) and PαMS which is the semiconductor and insulating polymer examined in this study, respectively. Note, μ_h denotes the hole mobility of the pure semiconductor, μ_h* denotes the mobility range for the semiconductor-insulating polymer blends, and μ_h# denotes the mobility of the blend for a semiconductor-insulating polymer weight ratio of 1:1.

A strategy to improve film morphology, degree of texture, solution processability, and thus charge transport of small molecules semiconductors, including *n*-(hetero)acenes, is by blending them with an insulating amorphous polymer.[38−45] To achieve high OFET performance the phase separation and crystallization of the small molecule/insulating polymer blend must be appropriately manipulated. In this strategy, *n*-(thio)acenes systems such as TIPS-PEN,[46] DiF-TESADT,[47] and C8-BTBT[48] (Figure 1b) blended with polystyrene (PS),[49−52] poly(α-methylstyrene) (PαMS),[47,53,54] or polyacrylate[55,56] binders have been widely investigated. For instance, pure TIPS-PEN exhibits a mobility of 1.8 cm^2 V^{-1} s^{-1}[46] which could be enhanced to 8.3 cm^2 V^{-1} s^{-1} for a 1:1 weight blend by optimizing formulation and coating parameters.[57] Similarly, DiF-TESADT[49,58,59] and C8-BTBT[51,60] mobilities could be increased from 1.5 cm^2 V^{-1} s^{-1}[47] and 1.8 cm^2 V^{-1} s^{-1}[48] for the pure systems, respectively, to 6.7 cm^2 V^{-1} s^{-1}[61] and 12 cm^2 V^{-1} s^{-1},[51] respectively, for the blend with a 1:1 weight ratio. Note, different blend ratios can strongly affect FET mobility which can vary from 0.103 to 8.3 cm^2 V^{-1} s^{-1} for TIPS-PEN/polymer blends,[54,57] from 1.9 to 6.7 cm^2 V^{-1} s^{-1} for DiF-TESADT/polymer blends,[49,61] and from 2 to 43 cm^2 V^{-1} s^{-1} for the C8-BTBT blends.[62] However, the limited stability of some of these molecular semiconductors persists in the blend and, unfortunately, the melting point of C8-BTBT is too low for stable device performance under thermal stress. Furthermore, the state-of-art blend-based OFETs were generally processed by spin-coating, which wastes most of the semiconductor formulation, and using highly toxic halogenated solvents. Additionally, it has been shown that charge carrier mobilities are strongly dependent upon the blend composition with the greatest performance achieved around the 1:1 weight ratio.[63−65] Thus, it would be desirable to investigate blends more forgiving to the polymer content variation and using more semiconductor saving processing methodologies.

In this paper we explore the blends of the molecular semiconductor **DDTT-DSDTT** (**1**) (Figure 1c), based on the **DSDTT** core. This molecule exhibits intramolecular locks using S···S interactions as accessed in previous studies on similar molecules[66] and established from the crystal structure. Compound **1** is a *p*-type organic semiconductor with a high hole mobility of 3.19 cm^2 V^{-1} s^{-1}; as per our knowledge, this is the highest reported to date within the all-thiophene semiconductor family. In addition, solution-sheared blends of **1** with the insulating polymer PαMS processed from the nonhalogenated solvent anisole exhibit a hole mobility of 2.44 cm^2 V^{-1} s^{-1} for the 50% molecule weight loading (1:1 weight ratio) and even 0.27 cm^2 V^{-1} s^{-1} for a 10% content. These results are rationalized by a combination of single crystal/electronic structure, physical, microstructural, and morphological characterizations.

Scheme 1. Synthetic Route to the Final Compound DDTT-DSDTT (1)

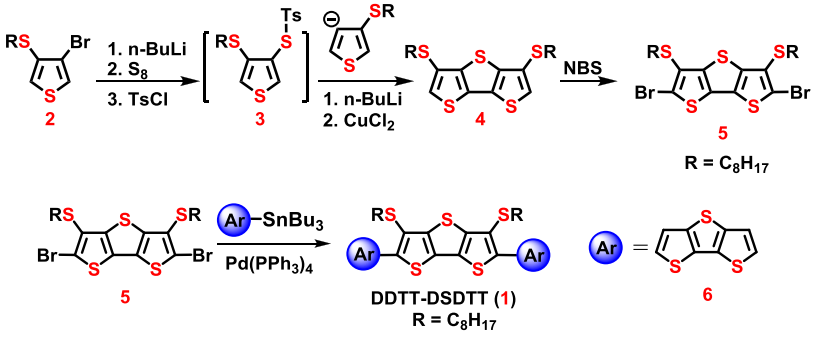

https://dx.doi.org/10.1021/acsnano.0c07003
ACS Nano 2021, 15, 727−738

RESULTS AND DISCUSSION

In this section, we first report the synthesis of **DDTT-DSDTT** (**1**) followed by evaluation of the structural and physical properties using several characterization techniques. Next, films and OFETs based on both the pristine and **1**/P*α*MS blends are fabricated using directional solution-shearing to reduce the materials costs as well as enhance the stability. Note, P*α*MS was selected because it has been previously used as a polymer binder mainly due to efficient phase separation and good environmental stability without sacrificing electrical performance.[65,67,68] Finally, the semiconductor film morphology and microstructure are characterized to rationalize the trends in mobilities as well as other physical properties.

Scheme 1 depicts the synthetic route to **DDTT-DSDTT** (**1**), and the main **DSDTT** (**4**) core was synthesized by the previously reported one-pot reaction method[66] from 3-bromo-4-thioalkylthiophene (**2**) in an overall yield of 15%. The DSDTT core was then brominated and next reacted with compound **6** to produce the small molecule **1** in good yield. Single crystals of molecule **1** were obtained to confirm the molecular structure and evidencing the planarity of the whole molecule (*vide infra*), which can contribute to the high charge transport performance of **1**. At the same time the two thiooctyl core substituents enable the good solubility of **1** in organic solvents, which is essential for fabricating the organic semiconductor films via solution processing. The thermal properties of compound **1** by differential scanning calorimetry (DSC, Figure S1) and thermogravimetric analysis (TGA, Figure S2) demonstrate a distinct melting transition at 184.8 °C and thermal stability up to 340 °C under a nitrogen atmosphere.

The UV−vis spectra of the **DSDTT** core and **DSDTT-DDTT** (**1**) in dilute *o*-dichlorobenzene solution are presented in Figure S3, and data are included in Table 1. The absorption maximum (λ_{max}) values of the **DSDTT** core and **1** in solution are located at 307 and 456 nm, respectively. As expected, with the **DSDTT** core end-functionalized with two aryl units, the absorption of molecule **1** was significantly red-shifted. We then investigated the optical properties of the **1**:P*α*MS blends both in solution and as thin films (Figure 2). The latter were fabricated on glass substrates using the same procedure carried out for OFET channel fabrication consisting of depositing a solution of **1**:P*α*MS in anisole (total concentration = 3 mg mL^{-1}, weight content of **1** vs P*α*MS going from 100% to 10%) by solution-shearing with a moving blade speed of 10 $\mu m\ s^{-1}$ on a heated substrate (60 °C). These films were next annealed at 70 °C for 2 h. In THF solution, compound **1** presents an intense absorption in the 400−500 nm region with a λ_{max} at 456 nm, and those of the **1**:P*α*MS blends are unchanged independently of the P*α*MS content. This result suggests that **1** solubility and aggregation in solution do not change when the insulating polymer is present. Neat **1** and its blend films display a significant bathochromic shift of the absorption compared to their solutions. Thus, pristine **1** films, as well as those of the blends, exhibit peaks at 447, 460, 491, and 529 nm, associated with well-defined (0−3), (0−2), (0−1), and (0−0) vibronic bands, respectively. Interestingly, for **1**:P*α*MS blend films, the intensities of the lower energy bands first increase when going from the pristine to the 50% **1** content in the blend films and then gradually decrease upon increasing the amounts of the P*α*MS. This result suggests that although the **1** content in the 80% and 50% blends is lower they exhibit a greater degree of aggregation, data consistent with the GIXRD data and supporting the considerable charge transport of these blends despite the reduced semiconductor content (*vide infra*). Estimated from the thin film absorption onset, the optical band gap of **1** is 2.13 eV which remains in the same range for all corresponding blends.

Table 1. Optical and Electrochemical Properties of DSDTT Core and DDTT-DSDTT (1)

compound	λ_{max}[a] (nm)	E_{ox}[b] (V)	E_{red}[b] (V)	HOMO[c] (eV)	LUMO[c] (eV)	E_g (eV)
DSDTT-core	307	1.27	n.d.	−5.47	−1.95[d]	3.52[e]
1	456	0.94	−1.70	−5.14	−2.50	2.64[f]

[a]In *o*-$C_6H_4Cl_2$. [b]In *o*-dichlorobenzene at 25 °C by DPV. All potentials are referenced to Fc/Fc^+ internal standard (at +0.6 V). [c]Using HOMO/LUMO = $-(4.2 + E_{ox}/E_{red})$. [d]Estimated from HOMO + E_g. [e]Optical energy gap was calculated using $1240/\lambda_{abs\ (onset)}$. [f]Obtained from DPV.

The electrochemical properties were measured by DPV in *o*-$C_6H_4Cl_2$ with a 0.1 M Bu_4NPF_6 solution at 25 °C. Note, DPV can more distinctively locate redox processes than conventional cyclic voltammetry (CV). The oxidation potential curves are shown in Figure 3a, and the calculated HOMO/LUMO energy levels of **DSDTT** and **1** are reported in Table 1 (see footnote for calculation details) and shown schematically in Figure 3b. The HOMO energy level of **DSDTT** and **1** is −5.47 and −5.14 eV, respectively. As expected, with the more aryl conjugated unit end-attached, the HOMO energy level of **1** is uplifted compared to the **DSDTT** core. The LUMO of **DSDTT** and **1** are −1.95 and −2.50 eV, respectively. Finally, density functional theory calculations at the B3LYP/6-31G (d) level (Figure S4) support energy trends and large delocalization of the frontier molecular orbitals over the whole molecules, which favor efficient charge transport.[69−71]

Single crystals of **1** were obtained by slow solvent evaporation of a hexane solution and the structure is shown in Figures 4 and S5. Compound **1** crystallizes in an orthorhombic *P*21/*c* space group. As shown in Figure 4a, the two thioalkylated chains are located on the same side of the central core. The short S(DTT)··S(R) distances (3.16 and 3.10 Å) depict the existence of an intramolecular nonbonded interaction between two sulfur atoms. Those distances are lesser than the sum of the van der Waals radii of two S atoms (3.60 Å). Front view of two stacking **DSDTT** molecules (Figure 4b) suggests that the **DSDTT** core and the two end-functionalized **DTT** groups are nearly coplanar, showing small dihedral angles of 1.73° and 1.96°. The shortest intermolecular stacking distance of two closely packed **DSDTT** molecules is 3.52 Å (Figure 4b and c). The stacking of molecule **1** exhibits a herringbone angle of 81.64° (Figure 4d) and also slipping angles of 40.37° and 67.51° (Figure 4e and f). In the columnar **DSDTT** molecule stacks, the smaller intermolecular S··S distances are 3.34−3.42 Å with a **DSDTT** core stacking distance of 3.52 Å (Figure 4g and h). These intra- and intermolecular short packing distances and the very planar structure of **1** crystal structure suggests good conditions for intra- and intermolecular $\pi-\pi$ orbital interaction to obtain highest charge transport results in the solid state.

Before OFET device fabrication, atomic force microscopy (AFM) and polarized optical microscopy (POM) imaging were carried out to investigate the blend morphology and

https://dx.doi.org/10.1021/acsnano.0c07003
ACS Nano 2021, 15, 727−738

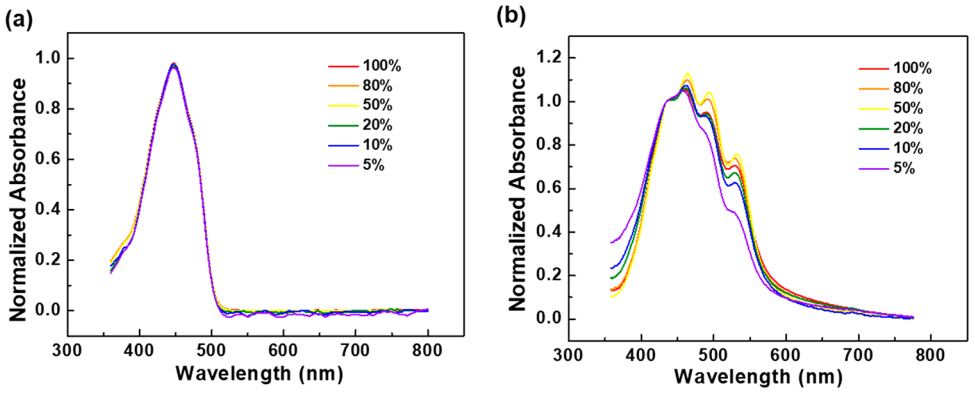

Figure 2. UV−vis absorption spectra of various 1:PαMS in (a) solution and (b) films.

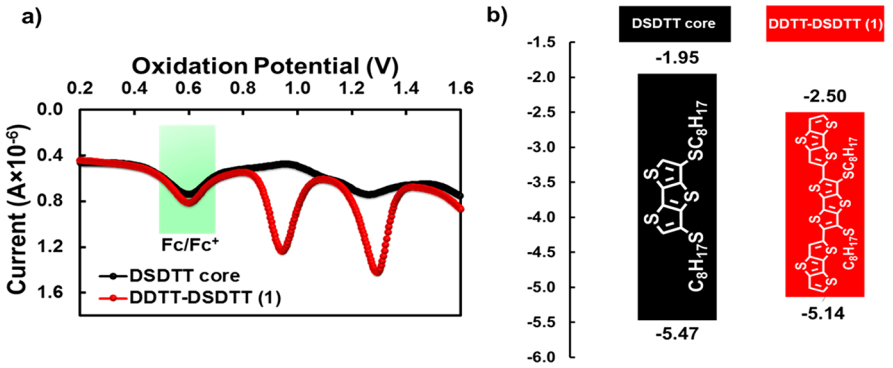

Figure 3. (a) DPV curves of DSDTT core and DDTT-DSDTT (1) in *o*-dichlorobenzene. (b) DPV-derived HOMO and LUMO energy levels.

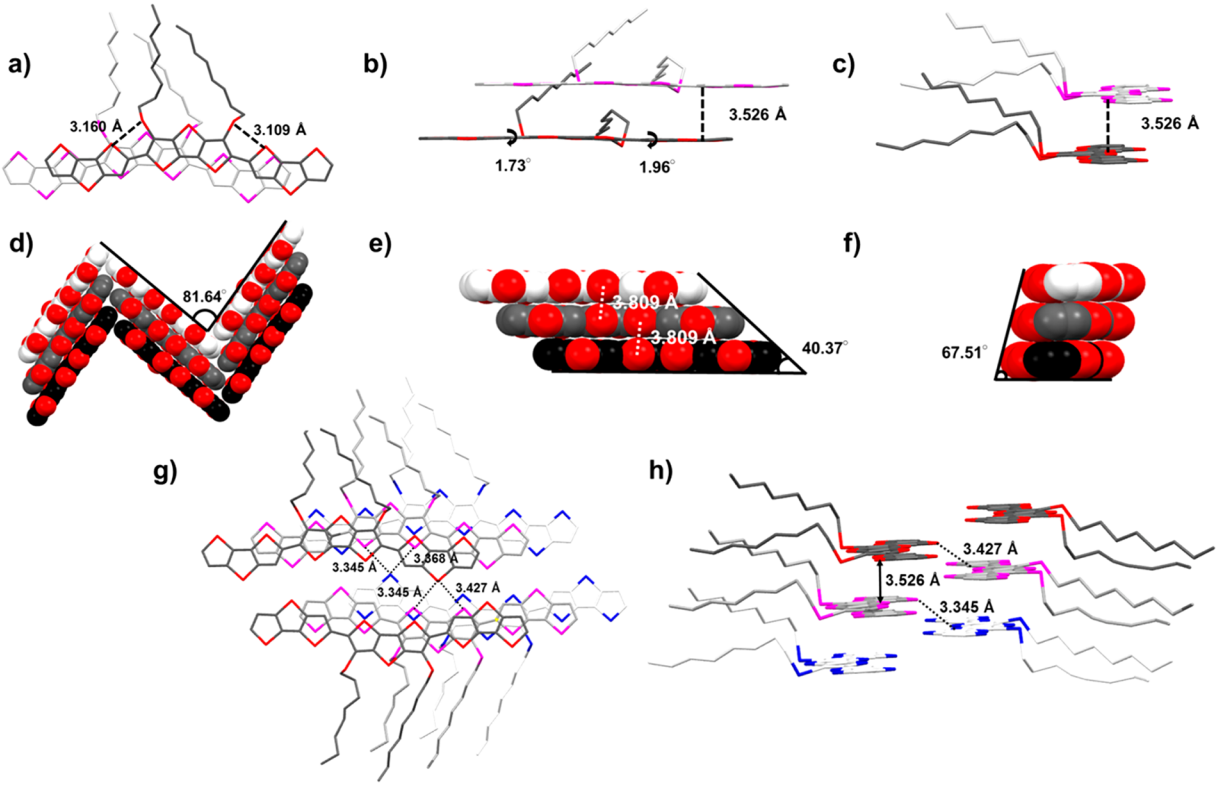

Figure 4. Single crystal structure of DDTT-DSDTT (1) in stick (a−c, g, h) and space filling models (d−f).

microstructural features of the solution-sheared blend films. The resulting topology as well as wide area POM images are shown in Figure 5a, 5c, 5e, 5g, 5i, and 5k. The film of pristine **1** shows well-interconnected microribbon-shaped crystals growing parallel to the shearing direction. The crystals almost fully cover the substrates, and few nonoriented crystal regions are

https://dx.doi.org/10.1021/acsnano.0c07003
ACS Nano 2021, 15, 727−738

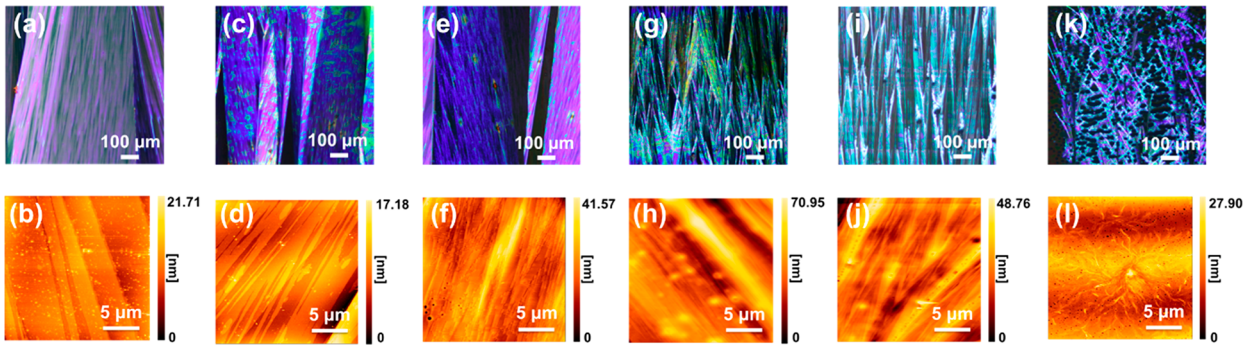

Figure 5. POM images (a, c, e, g, i, and k) and AFM topographies (b, d, f, h, j, and l) of blend thin films. The compound 1 composition in blend thin films: (a, b) 100%, (c, d) 80%, (e, f) 50%, (g, h) 20%, (i, j) 10%, and (k, l) 5%.

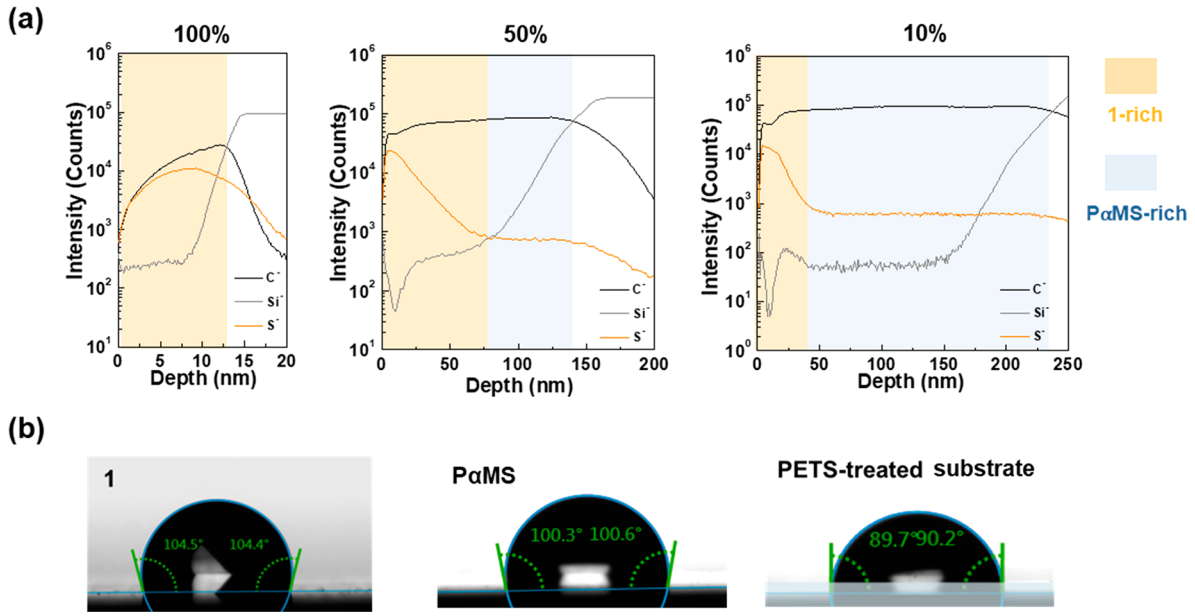

Figure 6. (a) Molecular depth profile measurements by TOF-SIMS in the compound 1 and 50% and 10% blend film. (b) Water contact angle of compound 1, PαMS, and PETS-treated surface.

observed (Figure 5a). The monotonic color indicates that the crystal thickness is rather uniform throughout the film. By blending with PαMS, the crystals are still continuous and oriented along the same axis, except for the 5% blend, but the crystal stripes are thinner. We suggest that the strong $\pi-\pi$ interactions between **1** molecules leads to the aligned 1D crystals under shear conditions even though **1** content is as low as 10%. As the fraction of **1** in the blend decreases to 5%, the semiconductor content is insufficient to form large crystals upon shearing, so that the blend film is discontinuous and the crystals are dendritic-like as well as nonoriented. The AFM images of the same films in Figure 5b, 5d, 5f, 5h, 5j, and 5l support the POM observation. The root-mean square-roughness of pristine **1** film is 2.54 nm, and it first increases to 2.58 nm (80%), 5.38 nm (50%), and 11.25 nm (20%) when the PαMS content increases from 20% to 80% and then it decreases to 7.21 nm (10%) and 4.13 nm (5%) for the largest polymer content. Thus, it appears that films fabricated with pristine **1** exhibit the best morphology for OFETs. These results also demonstrate that a small amount of **1** in the blends (~10%) is sufficient to provide sufficient pathways for efficient hole transport.

It has been shown that vertical phase separation in semiconductor-insulating polymer blends with even a low level of content of the semiconductor can provide a continuous transporting layer between source–drain electrodes, thus, achieving fully functional OFETs.[38−43] This result is due to considerable aggregation of high-performance molecular semiconductors.[45] For instance, it was found that the vertical separation of diF-TES-ADT (semiconductor)/PMMA blends (1:1 w/w) prevents dewetting of the F-TESADT film and provides a platform for diF-TES-ADT to crystallize at the air–film interface, thus enabling a field effect mobility of ~ 0.1 $cm^2 V^{-1} s^{-1}$.[64] TOF-SIMS measurements were carried out for the pristine compound **1** (control) as well as the 50% and 10% blend films to access possible vertical phase separation. Figure 6 shows the Poisson corrected ion signals plotted as a function of depth from the film/air interface. S and Si signals are makers for compound **1** and SiO_2, respectively. For the pristine **1** film, the data reveal that the semiconductor layer covers the Si/SiO_2 substrate. For the 50% blend film, the S signal decreases while the Si signal increases as the depth increases, indicating that **1** accumulates to the interface with the air; i.e., a vertical phase separation occurs forming a **1**-rich layer on the top side of the film while the bottom interface is PαMS-rich. The TOF-SIMS

https://dx.doi.org/10.1021/acsnano.0c07003
ACS Nano 2021, 15, 727−738

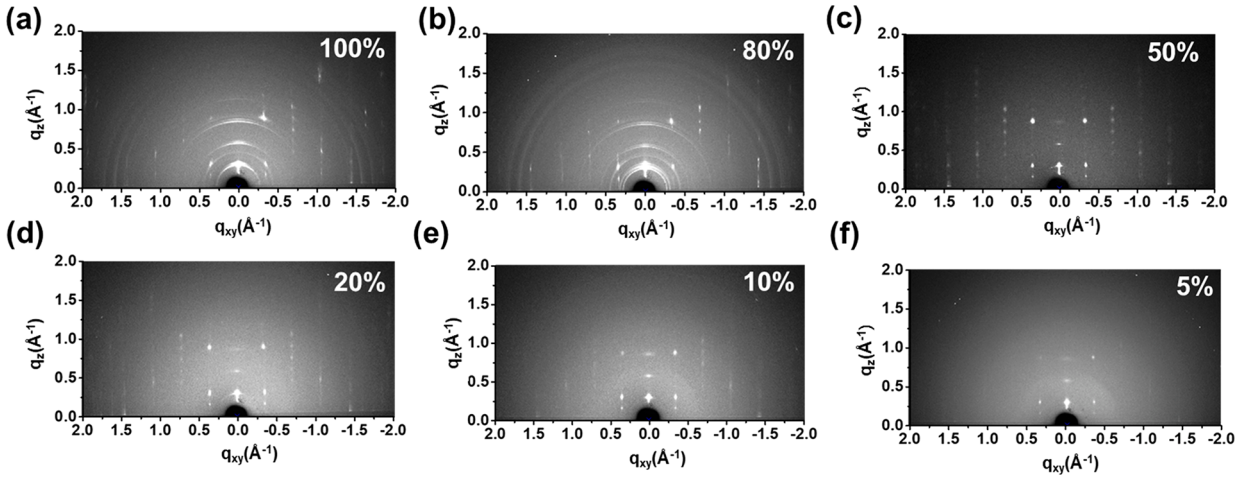

Figure 7. GIXRD patterns of blend thin film. The compound 1 composition in blend thin films: (a) 100%, (b) 80%, (c) 50%, (d) 20%, (e) 10%, and (f) 5%.

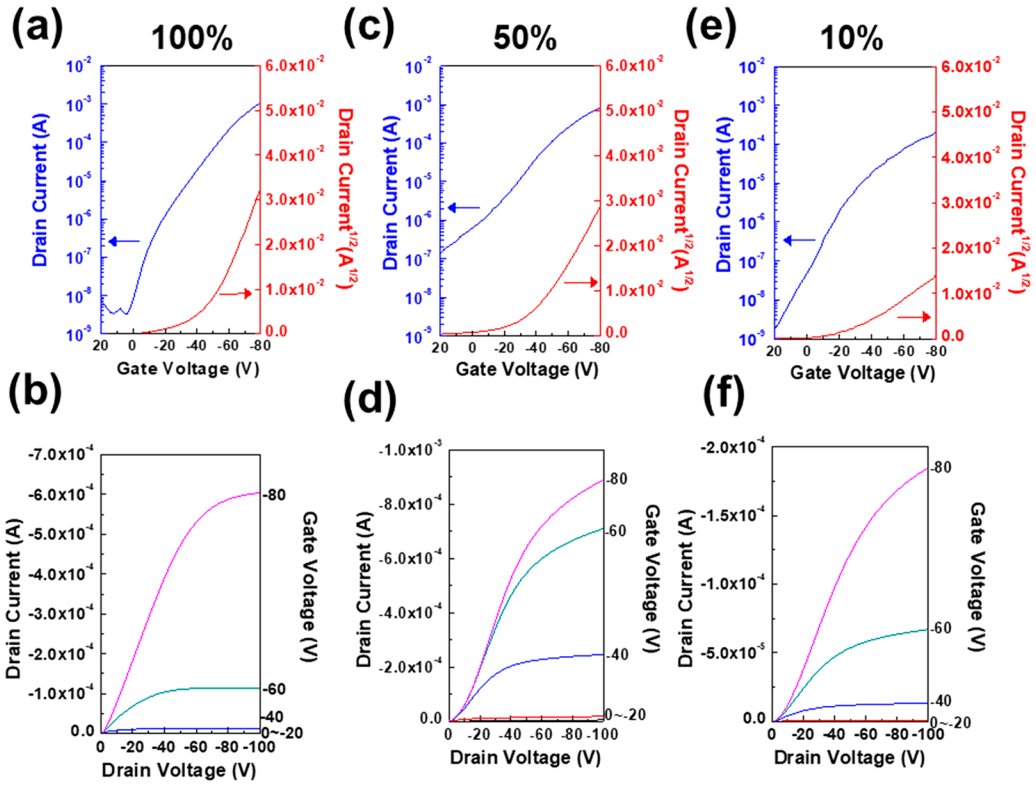

Figure 8. Transfer (a, c, and e; V_g sweep from 20 to −80 V with a fixed V_d of −100 V) and output characteristics (b, d, and f; V_d sweep from 0 to −100 V with a varied V_g from 0 to −100 V, in a step of −20 V) of blend OFETs device. The compound 1 composition in blend thin films: (a, b) 100%, (c, d) 50%, and (e, f) 10%.

data of the 10% blend film show an even sharper **1**-rich layer on top of the film. The estimated thickness of the vertically separated **1** and PαMS layers for the 50% blend is ∼75 and ∼65 nm, respectively, and thus the **1** weight content calculated from these thickness values is ∼52%, which is quite close to the original loading composition in the blend solution. Note that the density of **1** and PαMS is 1.01 (estimated from single crystal data) and 1.08 g mL^{-1}, respectively. For the 10% blend the layer thickness was found to be ∼40 nm for **1** and ∼200 nm for PαMS layer corresponding to ∼16% of **1** in the blend, again quite close to the 10% original loading. In a recent report, Cho's group suggested that gap-induced crystallization achieved by bar-coating, zone-casting, and solution-shearing methods can promote efficient vertical self-stratified structures in blend systems.[72] Contact angle measurements shown in Figure 6b indicate that **1** film is more hydrophobic (∼104.5°) than that of PαMS (∼100.5°), implying a lower surface free energy of **1** as compared to PαMS. This result further rationalizes why **1** and PαMS prefer to accumulate at the interface with the air and substrate, respectively.

Grazing incident X-ray diffraction (GIXRD) measurements were carried out for all films to examine the film texturing, molecular packing, and orientation (Figure 7). Diffraction patterns were obtained with the incident X-ray beam parallel to

https://dx.doi.org/10.1021/acsnano.0c07003
ACS Nano 2021, 15, 727−738

the solution-shearing direction at an incidence angle of 0.2°. Strong (00*l*) lamellar peaks along the out-of-plane direction (q_z) were observed for the pristine **1** film. A *d*-spacing of ~21.6 Å is measured from the (001) peak at q_z = 0.29 Å^{-1}, corresponding to the *c*-axis length of the unit cell. In the in-plane direction, the (10*l*) peak at q_{xy} = 1.37 Å^{-1} corresponds to a $\pi-\pi$ distance of 4.58 Å. The GIXRD results reveal that **1** molecule crystalline domains have the **DSDTT** molecular core aligned vertically with respect to the substrate surface, i.e. a preferential edge-on orientation. The stimulated packing motifs from the single crystal data exhibit a herringbone packing mode, with a face-to-face stacking within molecular columns and face-to-edge interactions between adjacent columns. This orientation is favorable for π-orbital overlap of neighboring molecules of **1** along parallel column directions, as well as for the lateral charge transport from one column to the adjacent one.[73−75] All blend films are also highly textured with pronounced lamellar scattering peaks up to the (003) out-of-plane direction reflections. The corresponding lattice spacings calculated from the (001) diffraction peaks are similar and between 21.8 and 22.1 Å. Thus, PαMS is extruded from the crystals of compound **1** and no new crystalline phases or solid solutions form. Among all blend films, the 50% one shows the sharpest (00*l*) reflections with respect to the central vertical line and several intense Bragg spots having less arc shape, featuring a high degree of crystal ordering and the texturing in spite of the reduced amount of semiconductor. Interestingly, the 50% blend film exhibits further improved film crystallinity as revealed by the increased diffraction intensity from the corresponding GIXRD line cuts in the (001) direction (Figure S5). These data are fully consistent with the intense (0−0) vibronic transition in the UV−vis absorption spectrum of this blend versus the other blends. Thus, an optimal amount of PαMS not only promotes alignment of **1** molecules and their packing along the direction perpendicular to the substrate but also enhances crystallinity. This is likely the result of two effects. We know that shear force is effective in promoting the sufficient amount of semiconductor.[76] Furthermore, it is also known that polymers can be aligned and aggregated more efficiently by shear force than small molecules.[77−79] Likely, the 50% blend contains a sufficient portion of semiconductor to create bulk crystals as well as sufficient polymer content so that the effect of shearing/aligning the polymer influences semiconductor crystal growth. For the 5% blend film, however, the diffraction peaks are weaker, which is due to the very low semiconductor content.

To investigate the electrical properties of the solution-sheared blend films as channel layers in OFETs, bottom-gate top-contact (BGTC) devices were fabricated on phenylethyltrichlorosilane (PETS)-modified SiO_2/n-doped Si substrate. The organic semiconducting blend films were solution-sheared as discussed in the UV−vis section. The devices were completed by thermal evaporation of the Au source and drain contacts through a shadow mask (channel length and width of 25 and 1500 μm, respectively). Figures 8 and S6 report representative transfer [drain voltage, V_d = −100 V] and output curves [gate voltage, V_g from 0 to −100 V] (both measured in dark/nitrogen conditions). The saturated field effect mobility values were extracted from the following equation

$$\mu = \frac{2L}{WC_i}\left(\frac{\partial\sqrt{I_d}}{\partial V_g}\right) \quad (1)$$

where C_i is the dielectric capacitance per unit area, and W and L are the width and length of channel, respectively. It should be noted that areal capacitance of the 300-nm-thick SiO_2 dielectric is estimated to be 11 nF cm^{-2} for field effect mobility calculation and the self-assembly monolayer modification does not affect the dielectric capacitance.[80] In addition, since the PαMS phase separates at the bottom interface and using the data provided by TOF-SIMS analysis, we have also estimated the mobility of the devices assuming that the gate capacitance decreases as a result of the formation of a nanoscopic PαMS layer on the SiO_2 dielectric (see Supporting Information for details). Based on these data, the corrected mobility of our blends are slightly larger than those using the pristine SiO_2 dielectric, in agreement with previous studies on other blends.[51,61,81] The calculated maximum and average mobility (μ_{max} and μ_{avg}) along with the threshold voltage (V_{th}) and current ON/OFF ratio ($I_{ON:OFF}$) are summarized in Table 2,

Table 2. OFET Device Parameters for the Indicated Blends

sample	max mobility [cm^2 V^{-1} s^{-1}]	average mobility [cm^2 V^{-1} s^{-1}]	$I_{ON:OFF}$	average V_{th} [V]
100%	3.19	1.30 ± 0.86	10^3−10^5	−18.0 ± 13.0
80%	2.76	1.20 ± 0.63	10^3−10^5	−21.4 ± 11.5
50%	2.44	0.74 ± 0.57	10^3−10^5	−13.8 ± 8.4
20%	0.55	0.16 ± 0.14	10^3−10^5	−36.9 ± 11.2
10%	0.27	0.15 ± 0.13	10^3−10^5	−24.4 ± 12.0
5%	0.09	0.03 ± 0.02	10^2−10^4	−32.5 ± 15.6

and device parameters (μ_{max}, μ_{avg}, and V_{th}) vs loading ratio of **1** in the blend are plotted in Figure S7. The OFET charge carrier mobility of the blends ranges from ~0.01 up to ~1 cm^2 V^{-1} s^{-1} and thus strongly depends on the **1**:PαMS ratios in the blends. Notably, the pristine **1** OFETs outperform all the other ones and exhibit a μ_{max} and μ_{avg} of 3.19 and 1.30 ± 0.86 cm^2 V^{-1} s^{-1}, while the 80% and 50% blend devices retain excellent charge transport with μ_{max} (μ_{avg}) amounting to 2.76 (1.20 ± 0.63) and 2.44 (0.74 ± 0.57) cm^2 V^{-1} s^{-1}, respectively. However, the mobility of the 20% and 10% blends decreases by ~10 × [μ_{max} (μ_{avg}) = 0.55 (0.16 ± 0.14) and 0.27 (0.15 ± 0.13) cm^2 V^{-1} s^{-1}, respectively] and diminishes even further, ~100 × [μ_{max} (μ_{avg}) = 0.09 (0.03 ± 0.02) cm^2 V^{-1} s^{-1}] for the 5% blend OFETs. The 50% blend films clearly exhibit highly ordered, homogeneous, and oriented crystallites with good interconnectivity. It is also evident that despite the high concentration of PαMS in the blend, efficient vertical phase separation occurs with crystallites on the top of a featureless surface of amorphous PαMS under the layer. A highly crystalline and interconnected layer forms also for the blends with a 10% semiconductor load as shown in the POM/AFM images (Figure 5i and 5j), thus, corroborating the lower, yet still efficient semiconducting properties. The significant drop in mobility for the 5% blends is due to both disruption in crystal connectivity and reduction of crystal size. The $I_{ON:OFF}$ of blend OFETs is 10^3−10^5 for the 10%−80% blend and pristine compound **1** with a slight decrease (1 order of magnitude) for the 5% blend. Note that the OFF current of these devices can be minimized; thus, the $I_{ON:OFF}$ increased, through patterning of the organic semiconductor and accurate patterning and registration of the semiconductor/gate electrode[82] as well as by

https://dx.doi.org/10.1021/acsnano.0c07003
ACS Nano 2021, 15, 727−738

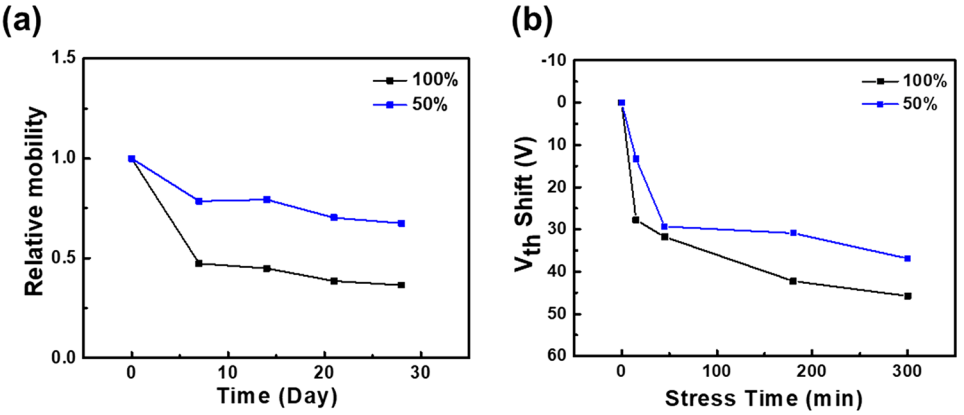

Figure 9. (a) Relative mobility as a function of exposure time to ambient air (room temperature, relative humidity = 50−60%) and (b) threshold voltage shift as a function of stress duration of pristine compound 1 and 50% blend films, following the V_g bias stress of −80 V with a V_d of −100 V. The transfer curves were measured at the following stress times: 0, 15, 45, 180, and 300 min.

optimizing the semiconductor thickness.[83] The average V_{th} varies in the range −13.8 ± 8.4 to −36.9 ± 11.2 V and shifts toward a more negative voltage for the lower organic semiconductor composition in the blend, since it requires a higher voltage to accumulate the mobile holes. Impressively, the 50% blend retains a mobility of ∼1 cm^2 V^{-1} s^{-1} but using far less semiconductor, potentially reducing the cost of the active layer of the device by ∼50%. Another important feature that should be emphasized here is that the reproducibility of all blend OFETs is significant. Since compound **1** and P*α*MS are immiscible, the blends phase separate into distinct nanometer-thick **1** and P*α*MS layers/domains in the transistor channel with the semiconductor (**1**) preferentially localizing at the air interface as evidenced by TOF-SIMS measurements. Thus, under the best conditions, compound **1** crystallizes in a nanoscaled space surrounded either by P*α*MS and air and the presence of the polymer promote formation of more ordered domains.[84] However, excessive polymer may result in surface contamination, which could create a thin polymer layer in-between the semiconductor and the top-contact electrodes, reducing charge injection efficiency. Thus, an ∼50% weight content seems to be a compromise between these two effects and the 50% blend enables enhanced crystallinity under shear and efficient charge injection.

The ambient and operational stability of OFETs is crucial for practical applications. Device performance deterioration in these devices has also been ascribed to interfacial traps which can be mitigated in terms of both bias stress[64,85,86] and ambient stability[68,85] when a polymer binder is used. To evaluate the device stability under ambient conditions, the fabricated OFETs were stored in highly humid air (relative humidity 50−60%) for 30 days. The corresponding relative mobility as a function of time is shown in Figure 9a, demonstrating that for 50% blend based OFETs the mobility declines far less than that of the devices based on the pristine **1**. Next, the operational stability of the same OFETs was accessed. The measured transfer curve and relative shifts of the extracted threshold voltage ($\triangle V_{th}$) over time (V_g = −80 V for 300 min) are given in Figures S9 and 9b, which reveals that the introduction of the insulating polymer in the blend decreases the $\triangle V_{th}$ under continuous bias stress. Our result can be also rationalized by the creation of a hydrophobic P*α*MS layer between the semiconductor and the gate dielectric reducing trap charge density at the semiconductor/dielectric interface.[60,62,87−89] Similar stability data have been shown for other important semiconductor/polymer blends such as those based on C8-BTBT[62] and a DNTT-precursor.[90] However, our blends offer a combination of a very high carrier mobility and complementary advantages such as processing from a green solvent, high thermal stability of the semiconductor, and low processing temperature for the blend film, the latter being needed for device fabrication of inexpensive plastic substrates.

CONCLUSION

In conclusion, we reported molecular semiconductor (**1**) and the corresponding **1**-insulating polymer blends and their incorporation into OFETs. Solution-sheared films of **1** from the environmentally friendly solvent (anisole) exhibit a carrier mobility as high as 3.19 cm^2 V^{-1} s^{-1} due to the highly coplanar DSDTT core, extended *π*-conjugation, and enhanced intermolecular cofacial *π*−*π* stacking. OFETs based on blend films retain very substantial charge transport properties for as much as 50% of insulating polymer content and exhibit a maximum hole mobility of 2.44 cm^2 V^{-1} s^{-1}. These devices also exhibit greater storage and bias stress stability versus those based on the pristine semiconductor film. The morphology/crystalline structure of blend films were also investigated corroborating nanoscopic vertical phase separation of **1**/P*α*MS and the presence of highly textured and connected semiconductor phases for as little as 10% of semiconductor content. Overall, our work contributes to the advancement of solution-processed small molecule-insulating polymer blends from environmentally acceptable solvents and the establishment of the correlation between the stratified crystalline structure and the electronic response of the corresponding OFETs.

METHODS

The synthetic details of organic semiconductors, materials, and characterization were described in the Supporting Information. OFET devices with bottom-gate top-contact (BGTC) configuration were fabricated on SiO_2/n-doped Si substrates (300 nm SiO_2 severing as dielectric). The blend active layer was deposited on the PETS-modified substrates by the solution-shearing technique with a previously reported setup[91,92] in ambient using a solution of **DDTT-DSDTT** (**1**) and P*α*MS in anisole (3 mg mL^{-1} total concentration) prepared at different **1**:P*α*MS weight ratios of 5:95, 10:90, 20:80. 50:50, 80:20, and 100:0. Afterward, the thin films were thermally annealed under vacuum at 70 °C for 2 h. Finally, the 60 nm Au source/drain electrodes were deposited by thermal evaporation

https://dx.doi.org/10.1021/acsnano.0c07003
ACS Nano 2021, 15, 727−738

using a shadow mask (channel length and width of 25 and 1500 μm, respectively). Electrical measurements were performed using a Keithley 4200-SCS semiconductor parameter analyzer in a glovebox. The ambient and operational stability tests were performed under air with high moisture (50−60%).

ASSOCIATED CONTENT

Supporting Information

The Supporting Information is available free of charge at https://pubs.acs.org/doi/10.1021/acsnano.0c07003.

Experimental details, DSC curves, TGA curves, absorption spectra, DFT calculation, single crystal structure, electrical characteristics, GIXRD, threshold voltage shifts, and NMR/HRMS spectra (PDF)

Crystallographic data for **DDTT-DSDTT** (**1**) (CIF)

AUTHOR INFORMATION

Corresponding Authors

Cheng-Liang Liu − *Department of Materials Science and Engineering, National Taiwan University, Taipei 10617, Taiwan;* orcid.org/0000-0002-8778-5386; Email: liucl@ntu.edu.tw

Ming-Chou Chen − *Department of Chemistry, National Central University, Taoyuan 32001, Taiwan;* orcid.org/0000-0001-9033-0131; Email: mcchen@ncu.edu.tw

Antonio Facchetti − *Department of Chemistry, Northwestern University, Evanston, Illinois 60208, United States;* orcid.org/0000-0002-8175-7958; Email: a-facchetti@northwestern.edu

Authors

Chia-Chi Lin − *Department of Chemical and Materials Engineering, National Central University, Taoyuan 32001, Taiwan*

Shakil N. Afraj − *Department of Chemistry, National Central University, Taoyuan 32001, Taiwan*

Arulmozhi Velusamy − *Department of Chemistry, National Central University, Taoyuan 32001, Taiwan*

Po-Chun Yu − *Department of Chemistry, National Central University, Taoyuan 32001, Taiwan*

Chang-Hui Cho − *Department of Chemistry, National Central University, Taoyuan 32001, Taiwan*

Jianhua Chen − *Department of Chemistry, Northwestern University, Evanston, Illinois 60208, United States;* orcid.org/0000-0002-4767-6310

Yi-Hsien Li − *Department of Chemistry, National Central University, Taoyuan 32001, Taiwan*

Gene-Hsiang Lee − *Instrumentation Center, National Taiwan University, Taipei 10617, Taiwan*

Shih-Huang Tung − *Institute of Polymer Science and Engineering, National Taiwan University, Taipei 10617, Taiwan;* orcid.org/0000-0002-6787-4955

Complete contact information is available at: https://pubs.acs.org/10.1021/acsnano.0c07003

Author Contributions

¶C.-C.L. and S.N.A. contributed equally to this work.

Notes

The authors declare no competing financial interest.

ACKNOWLEDGMENTS

C.-L.L. thanks for the funding from the Young Scholar Fellowship Program (Columbus Program) by MOST in Taiwan, under Grant MOST 109-2636-E-002-029. M.-C.C. thanks to MOST (MOST 109-3111-8-008-001) and NCU-DSM Research Center, and Research Center of New Generation Light Driven Photovoltaic Module for funding support. A.F. thanks to AFOSR (Grant FA9550-18-1-0320). The authors thanks to Beamline B13A1/B17A1/B23A1 from NSRRC of Taiwan for providing beamtime.

REFERENCES

(1) Sirringhaus, H. Reliability of Organic Field-Effect Transistors. *Adv. Mater.* **2009**, *21*, 3859−3873.

(2) Gelinck, G.; Heremans, P.; Nomoto, K.; Anthopoulos, T. D. Organic Transistors in Optical Displays and Microelectronic Applications. *Adv. Mater.* **2010**, *22*, 3778−3798.

(3) Braga, D.; Horowitz, G. High-Performance Organic Field-Effect Transistors. *Adv. Mater.* **2009**, *21*, 1473−1486.

(4) Mannsfeld, S. C. B.; Tee, B. C. K.; Stoltenberg, R. M.; Chen, C. V. H. H.; Barman, S.; Muir, B. V. O.; Sokolov, A. N.; Reese, C.; Bao, Z. Highly Sensitive Flexible Pressure Sensors with Microstructured Rubber Dielectric Layers. *Nat. Mater.* **2010**, *9*, 859−864.

(5) Zhao, Y.; Di, C.-a.; Gao, X.; Hu, Y.; Guo, Y.; Zhang, L.; Liu, Y.; Wang, J.; Hu, W.; Zhu, D. All-Solution-Processed, High-Performance n-Channel Organic Transistors and Circuits: Toward Low-Cost Ambient Electronics. *Adv. Mater.* **2011**, *23*, 2448−2453.

(6) Uno, M.; Cha, B.-S.; Kanaoka, Y.; Takeya, J. High-Speed Organic Transistors with Three-Dimensional Organic Channels and Organic Rectifiers Based on Them Operating above 20 MHz. *Org. Electron.* **2015**, *20*, 119−124.

(7) Natali, M.; Quiroga, S. D.; Passoni, L.; Criante, L.; Benvenuti, E.; Bolognini, G.; Favaretto, L.; Melucci, M.; Muccini, M.; Scotognella, F.; Di Fonzo, F.; Toffanin, S. Simultaneous Tenfold Brightness Enhancement and Emitted-Light Spectral Tunability in Transparent Ambipolar Organic Light-Emitting Transistor by Integration of High-k Photonic Crystal. *Adv. Funct. Mater.* **2017**, *27*, 1605164.

(8) Teshima, Y.; Saito, M.; Fukuhara, T.; Mikie, T.; Komeyama, K.; Yoshida, H.; Ohkita, H.; Osaka, I. Dithiazolylthienothiophene Bisimide: A Novel Electron-Deficient Building Unit for *n*-Type Semiconducting Polymers. *ACS Appl. Mater. Interfaces* **2019**, *11*, 23410−23416.

(9) Han, H.; Lee, C.; Kim, H.; Kim, Y. Flexible Near-Infrared Plastic Phototransistors with Conjugated Polymer Gate-Sensing Layers. *Adv. Funct. Mater.* **2018**, *28*, 1800704.

(10) Wang, Y.; Guo, H.; Harbuzaru, A.; Uddin, M. A.; Arrechea-Marcos, I.; Ling, S.; Yu, J.; Tang, Y.; Sun, H.; López Navarrete, J. T.; Ortiz, R. P.; Woo, H. Y.; Guo, X. (Semi)ladder-Type Bithiophene Imide-Based All-Acceptor Semiconductors: Synthesis, Structure−Property Correlations, and Unipolar *n*-Type Transistor Performance. *J. Am. Chem. Soc.* **2018**, *140*, 6095−6108.

(11) Wang, Y.; Guo, H.; Ling, S.; Arrechea-Marcos, I.; Wang, Y.; López Navarrete, J. T.; Ortiz, R. P.; Guo, X. Ladder-Type Heteroarenes: Up to 15 Rings with Five Imide Groups. *Angew. Chem., Int. Ed.* **2017**, *56*, 9924−9929.

(12) Fukuda, K.; Takeda, Y.; Yoshimura, Y.; Shiwaku, R.; Tran, L. T.; Sekine, T.; Mizukami, M.; Kumaki, D.; Tokito, S. Fully-Printed High-Performance Organic Thin-Film Transistors and Circuitry on One-Micron-Thick Polymer Films. *Nat. Commun.* **2014**, *5*, 4147.

(13) Zhang, C.; Zang, Y.; Gann, E.; McNeill, C. R.; Zhu, X.; Di, C.-a.; Zhu, D. Two-Dimensional π-Expanded Quinoidal Terthiophenes Terminated with Dicyanomethylenes as *n*-Type Semiconductors for High-Performance Organic Thin-Film Transistors. *J. Am. Chem. Soc.* **2014**, *136*, 16176−16184.

(14) Sekitani, T.; Zschieschang, U.; Klauk, H.; Someya, T. Flexible Organic Transistors and Circuits with Extreme Bending Stability. *Nat. Mater.* **2010**, *9*, 1015−1022.

(15) Vegiraju, S.; Hsieh, C.-M.; Huang, D.-Y.; Chen, Y.-C.; Priyanka, P.; Ni, J.-S.; Esya, F. A.; Kim, C.; Yau, S. L.; Chen, C.-P.; Liu, C.-L.; Chen, M.-C. Synthesis and Characterization of Solution-Processable Diketopyrrolopyrrole (DPP) and Tetrathienothiophene (TTA)-Based Small Molecules for Organic Thin Film Transistors and Organic Photovoltaic Cells. *Dyes Pigm.* **2016**, *133*, 280−291.
(16) Chakravarthi, N.; Gunasekar, K.; Cho, W.; Long, D. X.; Kim, Y.-H.; Song, C. E.; Lee, J.-C.; Facchetti, A.; Song, M.; Noh, Y.-Y.; Jin, S.-H. A Simple Structured and Efficient Triazine-Based Molecule as an Interfacial Layer for High Performance Organic Electronics. *Energy Environ. Sci.* **2016**, *9*, 2595−2602.
(17) Fei, Z.; Chen, L.; Han, Y.; Gann, E.; Chesman, A. S. R.; McNeill, C. R.; Anthopoulos, T. D.; Heeney, M.; Pietrangelo, A. Alternating 5,5-Dimethylcyclopentadiene and Diketopyrrolopyrrole Copolymer Prepared at Room Temperature for High Performance Organic Thin-Film Transistors. *J. Am. Chem. Soc.* **2017**, *139*, 8094−8097.
(18) Wang, C.; Dong, H.; Hu, W.; Liu, Y.; Zhu, D. Semiconducting π-Conjugated Systems in Field-Effect Transistors: A Material Odyssey of Organic Electronics. *Chem. Rev.* **2012**, *112*, 2208−2267.
(19) Takimiya, K.; Shinamura, S.; Osaka, I.; Miyazaki, E. Thienoacene-Based Organic Semiconductors. *Adv. Mater.* **2011**, *23*, 4347−4370.
(20) Takimiya, K.; Osaka, I.; Mori, T.; Nakano, M. Organic Semiconductors Based on [1]Benzothieno[3,2-b][1]benzothiophene Substructure. *Acc. Chem. Res.* **2014**, *47*, 1493−1502.
(21) Xue, G.; Fan, C.; Wu, J.; Liu, S.; Liu, Y.; Chen, H.; Xin, H. L.; Li, H. Ambipolar Charge Transport of TIPS-Pentacene Single-Crystals Grown from Non-Polar Solvents. *Mater. Horiz.* **2015**, *2*, 344−349.
(22) James, D. I.; Wang, S.; Ma, W.; Hedström, S.; Meng, X.; Persson, P.; Fabiano, S.; Crispin, X.; Andersson, M. R.; Berggren, M.; Wang, E. High-Performance Hole Transport and Quasi-Balanced Ambipolar OFETs Based on D−A−A Thieno-Benzo-Isoindigo Polymers. *Adv. Electron. Mater.* **2016**, *2*, 1500313.
(23) Wang, S.; Sun, H.; Ail, U.; Vagin, M.; Persson, P. O. Å.; Andreasen, J. W.; Thiel, W.; Berggren, M.; Crispin, X.; Fazzi, D.; Fabiano, S. Thermoelectric Properties of Solution-Processed n-Doped Ladder-Type Conducting Polymers. *Adv. Mater.* **2016**, *28*, 10764−10771.
(24) Mamillapalli, N. C.; Vegiraju, S.; Priyanka, P.; Lin, C.-Y.; Luo, X.-L.; Tsai, H.-C.; Hong, S.-H.; Ni, J.-S.; Lien, W.-C.; Kwon, G.; Yau, S. L.; Kim, C.; Liu, C.-L.; Chen, M.-C. Solution-Processable End-Functionalized Tetrathienoacene Semiconductors: Synthesis, Characterization and Organic Field Effect Transistors Applications. *Dyes Pigm.* **2017**, *145*, 584−590.
(25) Do, T.-T.; Takeda, Y.; Manzhos, S.; Bell, J.; Tokito, S.; Sonar, P. Naphthalimide End Capped Anthraquinone Based Solution-Processable n-Channel Organic Semiconductors: Effect of Alkyl Chain Engineering on Charge Transport. *J. Mater. Chem. C* **2018**, *6*, 3774−3786.
(26) Mei, J.; Diao, Y.; Appleton, A. L.; Fang, L.; Bao, Z. Integrated Materials Design of Organic Semiconductors for Field-Effect Transistors. *J. Am. Chem. Soc.* **2013**, *135*, 6724−6746.
(27) Wu, J.; Li, Q.; Xue, G.; Chen, H.; Li, H. Preparation of Single-Crystalline Heterojunctions for Organic Electronics. *Adv. Mater.* **2017**, *29*, 1606101.
(28) Fan, C.; Zoombelt, A. P.; Jiang, H.; Fu, W.; Wu, J.; Yuan, W.; Wang, Y.; Li, H.; Chen, H.; Bao, Z. Solution-Grown Organic Single-Crystalline p-n Junctions with Ambipolar Charge Transport. *Adv. Mater.* **2013**, *25*, 5762−5766.
(29) Vegiraju, S.; Huang, D.-Y.; Priyanka, P.; Li, Y.-S.; Luo, X.-L.; Hong, S.-H.; Ni, J.-S.; Tung, S.-H.; Wang, C.-L.; Lien, W.-C.; Yau, S. L.; Liu, C.-L.; Chen, M.-C. High Performance Solution-Processable Tetrathienoacene (TTAR) Based Small Molecules for Organic Field Effect Transistors (OFETs). *Chem. Commun.* **2017**, *53*, 5898−5901.
(30) Jiang, W.; Li, Y.; Wang, Z. Heteroarenes as High Performance Organic Semiconductors. *Chem. Soc. Rev.* **2013**, *42*, 6113−6127.
(31) Di Maria, F.; Olivelli, P.; Gazzano, M.; Zanelli, A.; Biasiucci, M.; Gigli, G.; Gentili, D.; D'Angelo, P.; Cavallini, M.; Barbarella, G. A Successful Chemical Strategy to Induce Oligothiophene Self-Assembly into Fibers with Tunable Shape and Function. *J. Am. Chem. Soc.* **2011**, *133*, 8654−8661.
(32) Salatelli, E.; Marinelli, M.; Lanzi, M.; Zanelli, A.; Dell'Elce, S.; Liscio, A.; Gazzano, M.; Di Maria, F. Bulk Heterojunction Solar Cells: The Role of Alkyl Side Chain on Nanoscale Morphology of Sulfur Over-Rich Regioregular Polythiophene/Fullerene Blends. *J. Phys. Chem. C* **2018**, *122*, 4156−4164.
(33) Xue, Z.; Chen, S.; Gao, N.; Xue, Y.; Lu, B.; Watson, O. A.; Zang, L.; Xu, J. Structural Design and Applications of Stereoregular Fused Thiophenes and Their Oligomers and Polymers. *Polym. Rev.* **2020**, *60*, 318−358.
(34) Cinar, M. E.; Ozturk, T. Thienothiophenes, Dithienothiophenes, and Thienoacenes: Syntheses, Oligomers, Polymers, and Properties. *Chem. Rev.* **2015**, *115*, 3036−3140.
(35) Shaw, C. M.; Zhang, X.; San Miguel, L.; Matzger, A. J.; Martin, D. C. Synthesis and Structure of α-Substituted Pentathienoacenes. *J. Mater. Chem. C* **2013**, *1*, 3686−3694.
(36) Xiao, K.; Liu, Y.; Qi, T.; Zhang, W.; Wang, F.; Gao, J.; Qiu, W.; Ma, Y.; Cui, G.; Chen, S.; Zhan, X.; Yu, G.; Qin, J.; Hu, W.; Zhu, D. A Highly π-Stacked Organic Semiconductor for Field-Effect Transistors Based on Linearly Condensed Pentathienoacene. *J. Am. Chem. Soc.* **2005**, *127*, 13281−13286.
(37) Liu, Y.; Sun, X.; Di, C.-a.; Liu, Y.; Du, C.; Lu, K.; Ye, S.; Yu, G. Hexathienoacene: Synthesis, Characterization, and Thin-Film Transistors. *Chem. - Asian J.* **2010**, *5*, 1550−1554.
(38) Scaccabarozzi, A. D.; Stingelin, N. Semiconducting:Insulating Polymer Blends for Optoelectronic Applications—A Review of Recent Advances. *J. Mater. Chem. A* **2014**, *2*, 10818−10824.
(39) Lee, W. H.; Park, Y. D. Organic Semiconductor/Insulator Polymer Blends for High-Performance Organic Transistors. *Polymers* **2014**, *6*, 1057−1073.
(40) Kang, B.; Ge, F.; Qiu, L.; Cho, K. Effective Use of Electrically Insulating Units in Organic Semiconductor Thin Films for High-Performance Organic Transistors. *Adv. Electron. Mater.* **2017**, *3*, 1600240.
(41) Smith, J.; Hamilton, R.; McCulloch, I.; Stingelin-Stutzmann, N.; Heeney, M.; Bradley, D. D. C.; Anthopoulos, T. D. Solution-Processed Organic Transistors Based on Semiconducting Blends. *J. Mater. Chem.* **2010**, *20*, 2562−2574.
(42) Jo, S. B.; Lee, W. H.; Qiu, L.; Cho, K. Polymer Blends with Semiconducting Nanowires for Organic Electronics. *J. Mater. Chem.* **2012**, *22*, 4244−4260.
(43) Riera-Galindo, S.; Leonardi, F.; Pfattner, R.; Mas-Torrent, M. Organic Semiconductor/Polymer Blend Films for Organic Field-Effect Transistors. *Adv. Mater. Technol.* **2019**, *4*, 1900104.
(44) Chou, L.-H.; Na, Y.; Park, C.-H.; Park, M. S.; Osaka, I.; Kim, F. S.; Liu, C.-L. Semiconducting Small Molecule/Polymer Blends for Organic Transistors. *Polymer* **2020**, *191*, 122208.
(45) Liu, C.; Li, Y.; Lee, M. V.; Kumatani, A.; Tsukagoshi, K. Self-Assembly of Semiconductor/Insulator Interfaces in One-Step Spin-Coating: A Versatile Approach for Organic Field-Effect Transistors. *Phys. Chem. Chem. Phys.* **2013**, *15*, 7917−7933.
(46) Park, S. K.; Jackson, T. N.; Anthony, J. E.; Mourey, D. A. High Mobility Solution Processed 6,13-Bis(triisopropyl-Silylethynyl) Pentacene Organic Thin Film Transistors. *Appl. Phys. Lett.* **2007**, *91*, No. 063514.
(47) Subramanian, S.; Park, S. K.; Parkin, S. R.; Podzorov, V.; Jackson, T. N.; Anthony, J. E. Chromophore Fluorination Enhances Crystallization and Stability of Soluble Anthradithiophene Semiconductors. *J. Am. Chem. Soc.* **2008**, *130*, 2706−2707.
(48) Ebata, H.; Izawa, T.; Miyazaki, E.; Takimiya, K.; Ikeda, M.; Kuwabara, H.; Yui, T. Highly Soluble [1]Benzothieno[3,2-b]-benzothiophene (BTBT) Derivatives for High-Performance, Solution-Processed Organic Field-Effect Transistors. *J. Am. Chem. Soc.* **2007**, *129*, 15732−15733.

https://dx.doi.org/10.1021/acsnano.0c07003
ACS Nano 2021, 15, 727−738

(49) Temiño, I.; Del Pozo, F. G.; Ajayakumar, M. R.; Galindo, S.; Puigdollers, J.; Mas-Torrent, M. A Rapid, Low-Cost, and Scalable Technique for Printing State-of-the-Art Organic Field-Effect Transistors. *Adv. Mater.* **2016**, *1*, 1600090.
(50) Tang, W.; Feng, L.; Yu, P.; Zhao, J.; Guo, X. Highly Efficient All-Solution-Processed Low-Voltage Organic Transistor with a Micrometer-Thick Low-k Polymer Gate Dielectric Layer. *Adv. Electron. Mater.* **2016**, *2*, 1500454.
(51) Haase, K.; Teixeira da Rocha, C.; Hauenstein, C.; Zheng, Y.; Hambsch, M.; Mannsfeld, S. C. B. High-Mobility, Solution-Processed Organic Field-Effect Transistors from C8-BTBT:Polystyrene Blends. *Adv. Electron. Mater.* **2018**, *4*, 1800076.
(52) Kim, K.; Hong, J.; Hahm, S. G.; Rho, Y.; An, T. K.; Kim, S. H.; Park, C. E. Facile and Microcontrolled Blade Coating of Organic Semiconductor Blends for Uniaxial Crystal Alignment and Reliable Flexible Organic Field-Effect Transistors. *ACS Appl. Mater. Interfaces* **2019**, *11*, 13481−13490.
(53) Seid, K. A.; Badot, J. C.; Dubrunfaut, O.; Levasseur, S.; Guyomard, D.; Lestriez, B. Multiscale Electronic Transport Mechanism and True Conductivities in Amorphous Carbon−LiFePO4 Nanocomposites. *J. Mater. Chem.* **2012**, *22*, 2641−2649.
(54) Jung, H. J.; Shin, Y. J.; Park, Y. J.; Yoon, S. C.; Choi, D. H.; Park, C. Ultrathin, Organic, Semiconductor/Polymer Blends by Scanning Corona-Discharge Coating for High-Performance Organic Thin-Film Transistors. *Adv. Funct. Mater.* **2010**, *20*, 2903−2910.
(55) Wang, Q.; Chen, T.; Li, M.; Zhang, B.; Lu, Y.; Chen, K. P. All-Fiber Ultrafast Thulium-Doped Fiber Ring Laser with Dissipative Soliton and Noise-Like Output in Normal Dispersion by Single-Wall Carbon Nanotubes. *Appl. Phys. Lett.* **2013**, *103*, No. 011103.
(56) Obata, S.; Miyazawa, Y.; Yamanaka, J.; Onojima, N. Environmentally-Friendly Fabrication of Organic Field-Effect Transistors Based on Small Molecule/Polymer Blend Prepared by Electrostatic Spray Deposition. *Jpn. J. Appl. Phys.* **2019**, *58*, SBBG02.
(57) Teixeira da Rocha, C.; Haase, K.; Zheng, Y.; Löffler, M.; Hambsch, M.; Mannsfeld, S. C. B. Solution Coating of Small Molecule/Polymer Blends Enabling Ultralow Voltage and High-Mobility Organic Transistors. *Adv. Electron. Mater.* **2018**, *4*, 1800141.
(58) Lee, W. H.; Lim, J. A.; Kwak, D.; Cho, J. H.; Lee, H. S.; Choi, H. H.; Cho, K. Semiconductor-Dielectric Blends: A Facile All Solution Route to Flexible All-Organic Transistors. *Adv. Mater.* **2009**, *21*, 4243−4248.
(59) Naden, A. B.; Loos, J.; MacLaren, D. A. Structure−Function Relations in DiF-TES-ADT Blend Organic Field Effect Transistors Studied by Scanning Probe Microscopy. *J. Mater. Chem. C* **2014**, *2*, 245−255.
(60) Pérez-Rodríguez, A.; Temiño, I.; Ocal, C.; Mas-Torrent, M.; Barrena, E. Decoding the Vertical Phase Separation and Its Impact on C8-BTBT/PS Transistor Properties. *ACS Appl. Mater. Interfaces* **2018**, *10*, 7296−7303.
(61) Niazi, M. R.; Li, R.; Qiang Li, E.; Kirmani, A. R.; Abdelsamie, M.; Wang, Q.; Pan, W.; Payne, M. M.; Anthony, J. E.; Smilgies, D.-M.; Thoroddsen, S. T.; Giannelis, E. P.; Amassian, A. Solution-Printed Organic Semiconductor Blends Exhibiting Transport Properties on Par with Single Crystals. *Nat. Commun.* **2015**, *6*, 8598.
(62) Yuan, Y.; Giri, G.; Ayzner, A. L.; Zoombelt, A. P.; Mannsfeld, S. C. B.; Chen, J.; Nordlund, D.; Toney, M. F.; Huang, J.; Bao, Z. Ultra-High Mobility Transparent Organic Thin Film Transistors Grown by an Off-Centre Spin-Coating Method. *Nat. Commun.* **2014**, *5*, 3005.
(63) Shin, N.; Kang, J.; Richter, L. J.; Prabhu, V. M.; Kline, R. J.; Fischer, D. A.; DeLongchamp, D. M.; Toney, M. F.; Satija, S. K.; Gundlach, D. J.; Purushothaman, B.; Anthony, J. E.; Yoon, D. Y. Vertically Segregated Structure and Properties of Small Molecule−Polymer Blend Semiconductors for Organic Thin-Film Transistors. *Adv. Funct. Mater.* **2013**, *23*, 366−376.
(64) Lee, W. H.; Kwak, D.; Anthony, J. E.; Lee, H. S.; Choi, H. H.; Kim, D. H.; Lee, S. G.; Cho, K. The Influence of the Solvent Evaporation Rate on the Phase Separation and Electrical Performances of Soluble Acene-Polymer Blend Semiconductors. *Adv. Funct. Mater.* **2012**, *22*, 267−281.
(65) Hamilton, R.; Smith, J.; Ogier, S.; Heeney, M.; Anthony, J. E.; McCulloch, I.; Veres, J.; Bradley, D. D. C.; Anthopoulos, T. D. High-Performance Polymer-Small Molecule Blend Organic Transistors. *Adv. Mater.* **2009**, *21*, 1166−1171.
(66) Vegiraju, S.; Luo, X.-L.; Li, L.-H.; Afraj, S. N.; Lee, C.; Zheng, D.; Hsieh, H.-C.; Lin, C.-C.; Hong, S.-H.; Tsai, H.-C.; Lee, G.-H.; Tung, S.-H.; Liu, C.-L.; Chen, M.-C.; Facchetti, A. Solution Processable Pseudo n-Thienoacenes *via* Intramolecular S···S Lock for High Performance Organic Field Effect Transistors. *Chem. Mater.* **2020**, *32*, 1422−1429.
(67) Shin, N.; Kang, J.; Richter, L. J.; Prabhu, V. M.; Kline, R. J.; Fischer, D. A.; DeLongchamp, D. M.; Toney, M. F.; Satija, S. K.; Gundlach, D. J.; Purushothaman, B.; Anthony, J. E.; Yoon, D. Y. Vertically Segregated Structure and Properties of Small Molecule−Polymer Blend Semiconductors for Organic Thin-Film Transistors. *Adv. Funct. Mater.* **2013**, *23*, 366−376.
(68) Zhong, H.; Smith, J.; Rossbauer, S.; White, A. J. P.; Anthopoulos, T. D.; Heeney, M. Air-Stable and High-Mobility n-Channel Organic Transistors Based on Small-Molecule/Polymer Semiconducting Blends. *Adv. Mater.* **2012**, *24*, 3205−3211.
(69) Lin, Z.; Liu, X.; Zhang, W.; Huang, J.; Wang, Q.; Shi, K.; Chen, Z.; Zhou, Y.; Wang, L.; Yu, G. Cyanostyrylthiophene-Based Ambipolar Conjugated Polymers: Synthesis, Properties, and Analyses of Backbone Fluorination Effect. *Macromolecules* **2018**, *51*, 966−976.
(70) Gao, Y.; Bai, J.; Sui, Y.; Han, Y.; Deng, Y.; Tian, H.; Geng, Y.; Wang, F. High Mobility Ambipolar Diketopyrrolopyrrole-Based Conjugated Polymers Synthesized *via* Direct Arylation Polycondensation: Influence of Thiophene Moieties and Side Chains. *Macromolecules* **2018**, *51*, 8752−8760.
(71) Fei, Z.; Han, Y.; Gann, E.; Hodsden, T.; Chesman, A. S. R.; McNeill, C. R.; Anthopoulos, T. D.; Heeney, M. Alkylated Selenophene-Based Ladder-Type Monomers *via* a Facile Route for High-Performance Thin-Film Transistor Applications. *J. Am. Chem. Soc.* **2017**, *139*, 8552−8561.
(72) Lee, S. B.; Kang, B.; Kim, D.; Park, C.; Kim, S.; Lee, M.; Lee, W. B.; Cho, K. Motion-Programmed Bar-Coating Method with Controlled Gap for High-Speed Scalable Preparation of Highly Crystalline Organic Semiconductor Thin Films. *ACS Appl. Mater. Interfaces* **2019**, *11*, 47153−47161.
(73) Yu, P.; Zhen, Y.; Dong, H.; Hu, W. Crystal Engineering of Organic Optoelectronic Materials. *Chem.* **2019**, *5*, 2814−2853.
(74) Yao, Z.-F.; Wang, J.-Y.; Pei, J. Control of $\pi-\pi$ Stacking *via* Crystal Engineering in Organic Conjugated Small Molecule Crystals. *Cryst. Growth Des.* **2018**, *18*, 7−15.
(75) Huang, C.-F.; Wu, S.-L.; Huang, Y.-F.; Chen, Y.-C.; Chang, S.-T.; Wu, T.-Y.; Wu, K.-Y.; Chuang, W.-T.; Wang, C.-L. Packing Principles for Donor−Acceptor Oligomers from Analysis of Single Crystals. *Chem. Mater.* **2016**, *28*, 5175−5190.
(76) Madec, M.-B.; Crouch, D.; Llorente, G. R.; Whittle, T. J.; Geoghegan, M.; Yeates, S. G. Organic Field Effect Transistors from Ambient Solution Processed Low Molar Mass Semiconductor−Insulator Blends. *J. Mater. Chem.* **2008**, *18*, 3230−3236.
(77) Shaw, L.; Hayoz, P.; Diao, Y.; Reinspach, J. A.; To, J. W. F.; Toney, M. F.; Weitz, R. T.; Bao, Z. Direct Uniaxial Alignment of a Donor−Acceptor Semiconducting Polymer Using Single-Step Solution Shearing. *ACS Appl. Mater. Interfaces* **2016**, *8*, 9285−9296.
(78) He, Z.; Zhang, Z.; Bi, S.; Chen, J.; Li, D. Conjugated Polymer Controlled Morphology and Charge Transport of Small-Molecule Organic Semiconductors. *Sci. Rep.* **2020**, *10*, 4344.
(79) Tamayo, A.; Riera-Galindo, S.; Jones, A. O. F.; Resel, R.; Mas-Torrent, M. Impact of the Ink Formulation and Coating Speed on the Polymorphism and Morphology of a Solution-Sheared Thin Film of a Blended Organic Semiconductor. *Adv. Mater. Interfaces* **2019**, *6*, 1900950.
(80) Halik, M.; Klauk, H.; Zschieschang, U.; Schmid, G.; Dehm, C.; Schütz, M.; Maisch, S.; Effenberger, F.; Brunnbauer, M.; Stellacci, F. Low-Voltage Organic Transistors with an Amorphous Molecular Gate Dielectric. *Nature* **2004**, *431*, 963−966.

https://dx.doi.org/10.1021/acsnano.0c07003
ACS Nano 2021, 15, 727−738

(81) Jo, P. S.; Duong, D. T.; Park, J.; Sinclair, R.; Salleo, A. Control of Rubrene Polymorphs *via* Polymer Binders: Applications in Organic Field-Effect Transistors. *Chem. Mater.* **2015**, *27*, 3979−3987.
(82) Lamport, Z. A.; Haneef, H. F.; Anand, S.; Waldrip, M.; Jurchescu, O. D. Tutorial: Organic Field-Effect Transistors: Materials, Structure and Operation. *J. Appl. Phys.* **2018**, *124*, No. 071101.
(83) Islam, M. N. Impact of Film Thickness of Organic Semiconductor on Off-State Current of Organic Thin Film Transistors. *J. Appl. Phys.* **2011**, *110*, 114906.
(84) Meldrum, F. C.; O'Shaughnessy, C. Crystallization in Confinement. *Adv. Mater.* **2020**, *32*, 2001068.
(85) Campos, A.; Riera-Galindo, S.; Puigdollers, J.; Mas-Torrent, M. Reduction of Charge Traps and Stability Enhancement in Solution-Processed Organic Field-Effect Transistors Based on a Blended *n*-Type Semiconductor. *ACS Appl. Mater. Interfaces* **2018**, *10*, 15952−15961.
(86) Kang, M.; Hwang, H.; Park, W.-T.; Khim, D.; Yeo, J.-S.; Kim, Y.; Kim, Y.-J.; Noh, Y.-Y.; Kim, D.-Y. Ambipolar Small-Molecule:-Polymer Blend Semiconductors for Solution-Processable Organic Field-Effect Transistors. *ACS Appl. Mater. Interfaces* **2017**, *9*, 2686−2692.
(87) Chen, M.-C.; Chiang, Y.-J.; Kim, C.; Guo, Y.-J.; Chen, S.-Y.; Liang, Y.-J.; Huang, Y.-W.; Hu, T.-S.; Lee, G.-H.; Facchetti, A.; Marks, T. J. One-Pot [1 + 1+1] Synthesis of Dithieno[2,3-b:3′,2′-d]thiophene (DTT) and their Functionalized Derivatives for Organic Thin-Film Transistors. *Chem. Commun.* **2009**, 1846−1848.
(88) del Pozo, F. G.; Fabiano, S.; Pfattner, R.; Georgakopoulos, S.; Galindo, S.; Liu, X.; Braun, S.; Fahlman, M.; Veciana, J.; Rovira, C.; Crispin, X.; Berggren, M.; Mas-Torrent, M. Single Crystal-Like Performance in Solution-Coated Thin-Film Organic Field-Effect Transistors. *Adv. Funct. Mater.* **2016**, *26*, 2379−2386.
(89) Georgakopoulos, S.; del Pozo, F. G.; Mas-Torrent, M. Flexible Organic Transistors Based on A Solution-Sheared PVDF Insulator. *J. Mater. Chem. C* **2015**, *3*, 12199−12202.
(90) Kimura, Y.; Nagase, T.; Kobayashi, T.; Hamaguchi, A.; Ikeda, Y.; Shiro, T.; Takimiya, K.; Naito, H. Soluble Organic Semiconductor Precursor with Specific Phase Separation for High-Performance Printed Organic Transistors. *Adv. Mater.* **2015**, *27*, 727−732.
(91) Vegiraju, S.; Chang, B.-C.; Priyanka, P.; Huang, D.-Y.; Wu, K.-Y.; Li, L.-H.; Chang, W.-C.; Lai, Y.-Y.; Hong, S.-H.; Yu, B.-C.; Wang, C.-L.; Chang, W.-J.; Liu, C.-L.; Chen, M.-C.; Facchetti, A. Intramolecular Locked Dithioalkylbithiophene-Based Semiconductors for High-Performance Organic Field-Effect Transistors. *Adv. Mater.* **2017**, *29*, 1702414.
(92) Vegiraju, S.; He, G.-Y.; Kim, C.; Priyanka, P.; Chiu, Y.-J.; Liu, C.-W.; Huang, C.-Y.; Ni, J.-S.; Wu, Y.-W.; Chen, Z.; Lee, G.-H.; Tung, S.-H.; Liu, C.-L.; Chen, M.-C.; Facchetti, A. Solution-Processable Dithienothiophenoquinoid (DTTQ) Structures for Ambient-Stable n-Channel Organic Field Effect Transistors. *Adv. Funct. Mater.* **2017**, *27*, 1606761.

https://dx.doi.org/10.1021/acsnano.0c07003
ACS Nano 2021, 15, 727−738